Available online at www.sciencedirect.com
ScienceDirect
Global and Planetary Change 59 (2007) 203–216
GLOBAL AND PLANETARY CHANGE
www.elsevier.com/locate/gloplacha

Influence of upper air conditions on the Patagonia icefields

L.A. Rasmussen [a,*], H. Conway [a], C.F. Raymond [a]

[a] *Department of Earth and Space Sciences, University of Washington Seattle, Washington 98195–1310, U.S.A.*

Available online 4 January 2007

Abstract

Upper-air conditions archived in the NCEP-NCAR Reanalysis have been used to investigate changes in precipitation and snowfall over the Patagonia icefields during 1960–99. Apparently, whereas total precipitation has not changed, warming has caused a decrease in the amount falling as snow. Precipitation at a site is taken to be proportional to the product of the relative humidity and the component of the wind in a particular critical direction, both at 850 hPa (~ 1400 m) at a point over the ocean to the west of the icefields; whether it falls as rain or snow is assumed to depend on whether the temperature at the elevation of the site is above or below +2 °C. The critical direction is assumed to be 270°, which is perpendicular to the north–south trending Andes and is also the prevailing wind direction in this zone of strong westerlies. Because of the scarcity of precipitation records on or near the icefields, the constant of proportionality cannot be determined, so the investigation is limited to examining relative changes in those upper air variables. Warming at 850 hPa has been ~ 0.5 °C over the 40 years, both winter and summer, with the effects that it has: (1) shifted from snow to rain ~ 5% of the precipitation, the total of which has changed little, and (2) increased annual melt in the ablation areas by ~ 0.5 m w.e. The icefields have been losing mass since at least 1870, so this 40-year trend represents only an acceleration of the longer-term trend of adjusting to climate change since the Little Ice Age.

Keywords: Patagonia; ice fields; glaciers; mass balance; upper-air

On the solid rock the ugly houses stand;
Come see my shining palace built upon the sand.

Edna St. Vincent Millay

1. Introduction

Until the past decade or two, the North Patagonia Icefield (NPI) and South Patagonia Icefield (SPI) have received little scientific attention compared with other bodies of ice in the world, yet they have made a substantial contribution to sea level rise, and interaction of ice with rivers and lakes has occasionally produced major floods (Casassa et al., 2002; Rivera et al., 2002; Rignot et al., 2003). Observations over the past 100 years have concentrated on changes at glacier termini, with only scant measurement of changes in ice thickness overall. The scarcity of climatological stations in the vicinity of the icefields, none of which make upper-air observations, and the total absence of stations for thousand of kilometers upwind in this zone of strong westerlies result in greater uncertainty in regional analyses of meteorological variables than elsewhere.

The icefields are in the zone of persistent midlatitude westerlies (Carrasco et al., 2002), which are slightly stronger in summer than in winter. They carry frequent

* Corresponding author.
E-mail address: LAR@geophys.washington.edu (L.A. Rasmussen).

0921-8181/$ - see front matter © 2006 Elsevier B.V. All rights reserved.
doi:10.1016/j.gloplacha.2006.11.025

cyclones from the Pacific Ocean against the substantial climate barrier created by the north–south trending Andes. The result is heavy precipitation on the west side and a sharp reduction of it on the lee side.

This investigation is conducted with upper-air data at 850 hPa (~ 1400 m above sea level) obtained from the NCEP–NCAR Reanalysis project (Kalnay et al., 1996; Kistler et al., 2001). That project, which is ongoing,

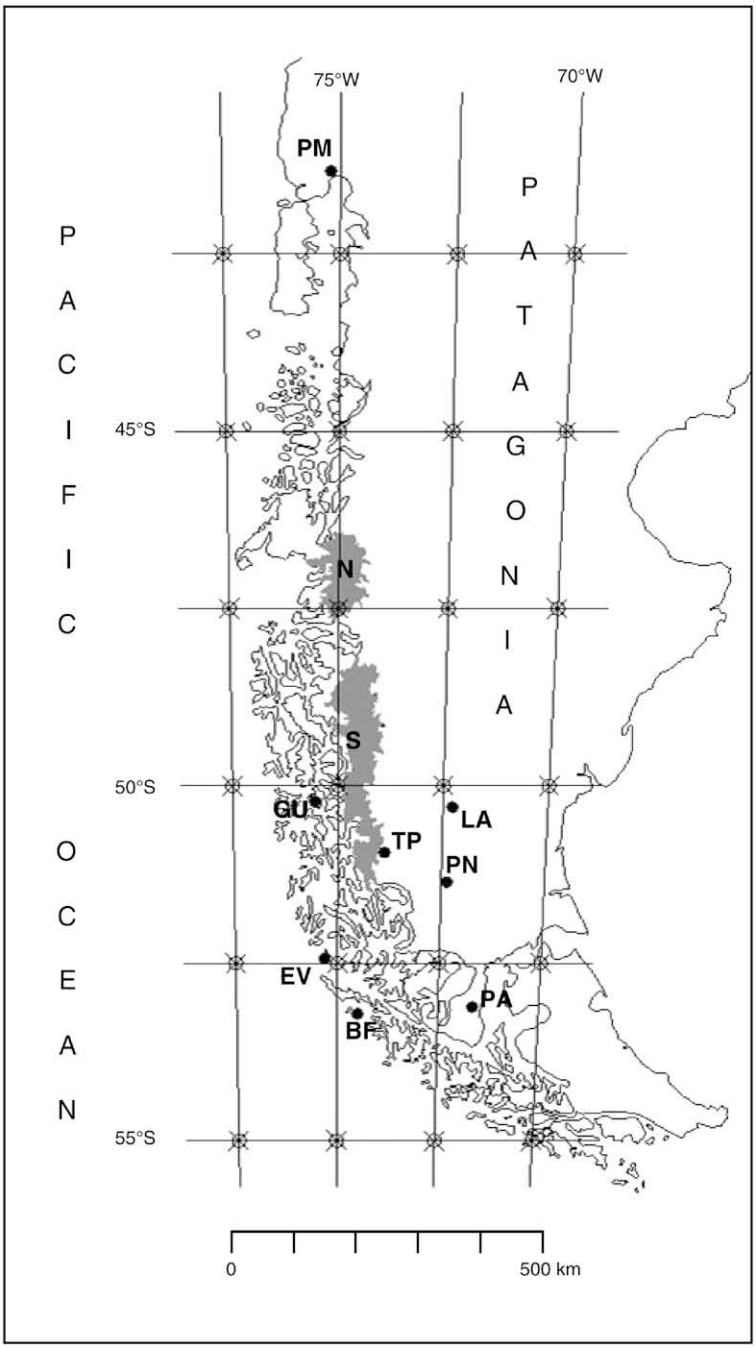

Fig. 1. Southern South America with NPI (N), SPI (S), and Reanalysis gridpoints (asterisks). Precipitation stations are Bahia Felix (BF), Evangelistas (EV), Guarello (GU) all at sea level; Lago Argentino, 220 m (LA); Punta Arenas, 34 m (PA); Puerto Montt, 110 m (PM); Puerto Natales (PN) and Torres del Paine (TP) both at 45 m.

systematically merges historically archived surface, radiosonde, and satellite observations to produce a set of internally consistent meteorological values interpolated at several vertical levels to a regular grid spanning the entire Earth. Daily values at 1200 UTC over 1948–99 are used at gridpoints equally spaced at six latitudes between 42.5° and 55°S, and four longitudes between 70°W and 77.5°W (Fig. 1).

Total precipitation over the Patagonia icefields is assumed to be related to 850-hPa wind and humidity in the same way as on the west coast of North America at about latitude 35°N (Pandey et al., 1999) and at about 48°N (Rasmussen et al., 2001; Rasmussen and Conway, 2001; Hayes et al., 2002). The model developed for the region at 48°N discerned whether precipitation at a given elevation fell as rain or snow by interpolating the temperature at that elevation between the 850 and 700-hPa (~ 3000 m) levels. The relations detected by those studies between snowfall and simple functions of upper-air variables are assumed to exist in other mid-latitude regions on the west coast of land barriers, which are zones of prevailing westerlies where most precipitation comes from extratropical cyclones moving onshore. In the absence of abundant measurements of mass balance on the icefields, as well as of precipitation at nearby sites, quantitative relations between snowfall and upper-air conditions cannot be calibrated in this region; instead, relative changes over time in snowfall are assumed to be proportional to relative changes in the relevant upper-air conditions.

2. The icefields

The elevation of most of the 4200-km^2 NPI is between 1000 and 1500 m. The 28 outlet glaciers that are greater than 5 km^2 in area terminate on land, except for San Rafael Glacier on the west side, which calves into Laguna San Rafael (Warren and Sugden, 1993). Equilibrium line altitude (ELA) is estimated for numerous individual NPI glaciers (Kerr and Sugden, 1994) by assuming that two-thirds of the glacier area lies above it. They estimate a mean ELA of ~ 700 m on the west side of NPI and ~ 1200 m on the east side.

The 13,000-km^2 SPI is composed of 48 major outlet glaciers and over 100 small cirque and valley glaciers (Aniya et al., 1996). All but two of the outlet glaciers calve, those on the west side into the sea, those on the east side into freshwater lakes between about 100 and 300 m in elevation. Because the ablation areas are truncated by calving, generally much less than one-third of the area of a glacier lies below its ELA. The observed ELA of 10 glaciers on the west side ranges between 800 and 1300 m, and of 13 on the east side between 650 and 1400 m (Casassa et al., 2002). The mean elevation of the SPI accumulation area is 1600 m.

Aniya et al. (2000) summarize recent changes in areal extent of outlet glaciers of both NPI and SPI. Harrison and Winchester (2000) found synchronous response of glaciers on the west and east sides of NPI with terminus-position retreat beginning in the 1870s, pausing in the mid-1900s, and resuming in the 1960s. Warren and Sugden (1993) ascribe similar retreat to SPI over the period but with several instances of individual glacier advances and less synchronous behavior between east and west. Detailed comparison from Landsat images of 34 glaciers terminating on land (Skvarca and De Angelis, 2002) showed that 33 retreated between 1986 and 2001.

Aniya and Wakao (1997) estimate that the 1945–96 volume decrease of the NPI was 264 ± 40 km^3 due mainly to thinning along with a slight amount due to retreat; over the icefield's 4200-km^2 area this averages 1.2 ± 0.2 m/a of thinning over the 51-year period. Rivera et al. (2002) estimate that NPI and the Chilean part of SPI, which is most of it, contributed an average of 0.032 ± 0.013 mm/a to sea level rise. This is a substantial fraction of the total contribution from all glaciers, which Dyurgerov and Meier (1997) estimate as 0.25 mm/a over 1961–90.

Mass balance measurements, especially of accumulation, are sparse. In recent years, ablation has been measured during summer on the lower reaches of a few NPI glaciers (Kobayashi and Saito, 1985; Ohata et al., 1985; Fukami and Naruse, 1987; Takeuchi et al., 1999;) and a few SPI glaciers (Koizumi and Naruse, 1992; Takeuchi et al., 1995; Naruse et al., 1997; Takeuchi et al., 1999). Average annual mass balance of 0.78 m w.e. over 1996–98 was measured at a 1460-m site on the east side of SPI (Casassa et al., 2002). Firn cores in accumulation areas yield mass balance information, but the few that have been obtained sample only the most recent few years. The cores do not exhibit a coherent pattern, perhaps in part because they undersample a variable with strong spatial and temporal variation, perhaps in part because of difficulty in interpreting the core stratigraphy.

Two firn cores in NPI are consistent with the expected east–west gradient of accumulation (Warren and Sugden, 1993; Hulton and Sugden, 1995). At a point on the west side, Yamada (1987) measured annual balance 3.45 m w.e. in 1985. At a point on the east side, Matsuoka and Naruse (1999) measured annual balance 2.2 m w.e. in 1996; the winter balance 3.5 m w.e. consisted entirely of accumulation, whereas the −1.3 m

w.e. summer balance was the resultant of 2.1 m w.e. accumulation offset by 3.4 m w.e. ablation.

A 13.2-m core obtained in September 1986 at 2680 m toward the southern end of SPI at 50.63°S, 73.25°W was interpreted by Aristarain and Delmas (1993) as showing 1.2 m w.e. average mass balance over the previous 5 years. This was only one-third of what they expected for the site according to other measurements in the vicinity. They speculated that wind scouring had removed much of the deposited snow, as reported at sites on NPI, but also acknowledged the possibility of mistakenly identifying annual layers in their core.

A 46.0-m core obtained in December 1999 at 1756 m on the accumulation area of Tyndall Glacier at 51°S in SPI (Godoi et al., 2002; Shiraiwa et al., 2002) showed an average of 14.4 m w.e. per year over the previous 2 years. Although the large value is almost double other determinations in the region, it is consistent with the 1.8 m w.e. accumulation during the 24 days when they were at the site.

Takeuchi et al. (1996) measured ablation of 6.3 m w.e. between 12 November 1993 and 1 March 1994 near the terminus of Moreno Glacier. They formed a linear relation between ablation and cumulative degree–day temperature over this period. By applying the relation to temperatures they measured from 1 December 1993 to 30 November 1994, they obtained an estimate of 12.8 m w.e. annual ablation.

Casassa et al. (2002) estimate mean annual mass balance for SPI of +6.7 m w.e. over 8700-km^2 of the accumulation area and −5.8 m w.e. over 4100-km^2 of the ablation area. The excess accumulation supplies a 35 km^3 mean annual volume to calving, which is equivalent to an average of 2.7 m over the total 13,000-km^2 area. Rignot et al., (2003) compared topography obtained by satellite in 2000 with earlier cartography and found thinning rates of SPI and NPI over 1995–2000 that were more than double the rates between about 1970 and 1995. They conclude that the acceleration of thinning is due to increased calving, as well as to climate forcing.

3. Precipitation measurements

Escobar et al. (1992) estimate mean annual precipitation of 6.7 meters averaged over NPI and 7.0 meters over SPI, along with evapotranspiration losses of only 4%. They give the spatial gradient as increasing from 6.4 m on the east side to 7.4 m on the west side of SPI, which is only about 20%. Carrasco et al. (2002), however, give a gradient for SPI of at least 50%.

Precipitation at weather stations near SPI has little seasonal variation compared with a station far to the north (Fig. 2). The strong westward-increasing gradient is manifested by the 11:1 ratio over 1961–70 between Bahia Felix and Punta Arenas (Fig. 1), where there was negligible seasonal variation of precipitation. Mercer (1965) reported an average of 7.5 meters per year at Guarello (Fig. 1) over a six-year period. Correlation of monthly precipitation between Puerto Natales and Torres Del Paine (Fig. 1) over 1980–2000 ranges from a low of $r=0.04$ in May to a high of $r=0.87$ in June, but is generally much lower than for stations separated by similar distances at 48°N (Table 2 of Rasmussen et al., 2001).

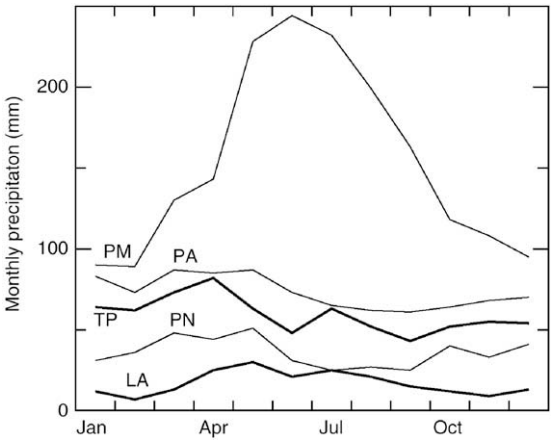

Fig. 2. Mean monthly precipitation in millimeters. Values averaged over 1982–2000 for Torres del Paine (TP), over 1985–2000 for Puerto Natales (PN). Values for Puerto Montt (PM), Punta Arenas (PA), and Lago Argentino (LA) from World Meteorological Organization, Monthly Climatic Data for the World.

Precipitation declined about 15% at Bahia Felix over 1915–1960 and 20% at nearby Islote Evangelistas over 1900–1950, with little change afterward until 1985 at either station (Rosenbluth et al., 1995). At Lago Argentino, where temperature trends were negligible in all seasons, precipitation declined about 20% over 1937–90, with the 1980s especially dry (Ibarzabal y DonAngelo et al., 1996). Rosenbluth et al. (1997) calculated a rise of mean temperature at surface stations in southern Patagonia of about 0.4°C per 100 years, most of it due to rise in minimum temperatures.

4. A simple snowfall model

A simple model (Rasmussen et al., 2001) estimates precipitation from

$$P^* = \alpha F \tag{1}$$

where α is an empirical constant and F is a pseudoflux given by

$$F = U\ \mathrm{RH} \tag{2}$$

in which $U = |\overrightarrow{V}_{850}|\cos(\phi_{850} - \phi')$ is the component of the 850-hPa wind in a critical direction ϕ' and $0 \le \mathrm{RH} \le 1$ is the 850-hPa relative humidity. Constraints $U > 2$ m/s (Hayes et al., 2002) or 3 m/s (Rasmussen et al., 2001), along with $\mathrm{RH} > 0.64$ were imposed for sites with westerly exposure on the west coast of North America to avoid estimating precipitation on days with weak onshore flow. If the constraints are not met, F is taken to be zero. The best-fitting direction ϕ' is determined empirically for a particular station from its existing precipitation record, and the yield factor α is calculated directly to optimize the goodness of fit, expressed by

$$r^2 = 1 - \left(\frac{\mathrm{rms}}{\sigma}\right)^2 \tag{3}$$

Here σ is the standard deviation of the observed precipitation P, and rms is the root mean square of the differences $P^* - P$. Because RH is dimensionless, F has units meters per second.

The quantity αF is used as an approximation of the divergence of the moisture flux, which corresponds directly (when the divergence is negative) to the amount of moisture removed from the air. This is done first on the assumption that when the flow is from the sector of ϕ', the negative divergence correlates strongly with F. Second is the assumption that F is a better indicator of precipitation potential than the true moisture flux $U e$, in which e is the vapor pressure or specific humidity, because precipitation is a saturation phenomenon. The third assumption is that the total flux in the vertical column correlates well with that at 850 hPa, which is used here because it is a standard level routinely reported and archived. This level usually carries more moisture than higher levels, yet is high enough to sample free-air conditions, and its wind is strongly correlated with winds at higher levels. These assumptions are consistent with conditions Pandey et al. (1999) analyzed in California.

Enomoto and Nakajima (1985) interpreted the strong correlation between precipitation over the southern Andes and the height of the 500 hPa level (~5500 m) over the Pacific Ocean in terms of the strength of the jet stream over the region. Schneider and Gies (2004) found the strength of the westerlies there to have moderate positive correlation with the Southern Oscillation Index, with the strength being smaller during El Niño periods.

Because of the scarcity of observations of snowfall in the region, it is not possible to make reliable assessments of model accuracy. Hulton and Sugden (1995) applied a vertically-integrated moisture-balance model to estimate snowfall over Patagonia. By comparison, the model used here is vastly simpler. In the northern hemisphere, however, where there is more abundant data, its results compared favorably with those from a widely used, powerful mesoscale model (Appendix A).

Measurements in 1957–58 at 2050 m on Blue Glacier indicated (Rasmussen et al., 2000) that temperature interpolated at that elevation between the 850 and 700-hPa levels in the radiosonde was a good indicator of whether precipitation fell on the glacier as rain ($T > +2$ °C) or snow ($T \le +2$ °C), which was also used by Oerlemans (1993). Other analyses (Laumann and Reeh, 1993; Johannesson et al., 1995) have used +1 °C as the rain–snow divide. Model results are not sensitive to the value of that parameter because if Eq. (1) is used to calculate precipitation flux, and then it is partitioned into snow or rain depending on whichever value is used, the regression coefficient in estimating snowfall at a site will adjust to accommodate changes in the amount of the flux classified as snow. Also, the time series of the part of it classified as snow upon using one value of the parameter will have relative changes over the period of record nearly the same as those from one formed using another value of it.

Blue glacier, 65 km inland from the radiosonde station on the coast, is at 48°N. Using temperatures at lowland stations is hampered by the great variability of the vertical lapse rate $\mathrm{d}T/\mathrm{d}z$. Temperatures at the glacier correlated much better with those from the radiosonde ($r^2 = 0.73$) than from a nearby lowland station (Forks) with an exceptionally good record ($r^2 = 0.19$).

Precipitation, including both solid and liquid forms, is assumed to be proportional to F, so it is referred to here as the precipitation flux and the part occurring when $T \le +2$ °C as the snow flux. Because of the covariance of precipitation and temperature and because of the nonlinear occurrence of the meteorological variables in Eq. (2), as well as in the discontinuity of the rain–snow discrimination, increments of both the precipitation flux and the snow flux are calculated daily. Values at 1200 UTC (0700 local time at longitude 75°W) are used to avoid day–night inhomogeneities (Section 5) in archived humidity values. Were monthly data used instead, the model would classify precipitation in a month either as all snow or as all rain.

In the development of the model, upper-air conditions were taken from the Quillayute radiosonde at 47.95°N, 124.55°W. It estimated precipitation well at sites with strong upslope exposure to the moisture-laden westerly winds. Although there are no long records from stations comparably sited west of the Patagonia icefields, the model did estimate precipitation at stations

with weaker upslope exposure to the westerlies — Puerto Montt, Torres del Paine, Puerto Natales, and Bahia Felix (Fig. 1) — but with accuracy substantially poorer than for stations in the 48°N region. Detailed results of four applications of the model at 48°N are given in Appendix A and Table A-1.

5. Comparisons of Reanalysis and radiosonde databases

Although applications of the model in North America used measurements from the radiosonde station at Quillayute, subsequent tests showed that data from the Reanalysis gridpoint 60 km to the SW at 47.5°N, 125°W gave similar results for 1966–96 applications of the model (Appendix A, Table A-1). In all cases, using both 0000 and 1200 UTC radiosondes gives results better than using only the one at 1200 UTC. When only 1200 UTC values are used, in some cases radiosonde data give slightly better results, sometimes Reanalysis data do.

There is a systematic difference over 1967–98 in the 850-hPa wind and humidity between the Quillayute radiosonde and the Reanalysis data (Table A-2 in the Appendix A). The Reanalysis humidity is lower, and the wind is more westerly and weaker. Moreover, the distribution of Reanalysis windspeeds and humidities on days when Forks had at least 10 mm precipitation is much narrower than the distribution of radiosonde values. Wet days at Forks are used as the criterion for concentrating on those days when precipitation in the nearby mountains is most likely. These are probably intrinsic differences in the two databases, rather than being due to the 60-km distance between the two locations.

In Patagonia, Carrasco et al. (2002) found correlation $r=0.98$ over 1977–98 between 850-hPa temperatures in the Punta Arenas radiosonde and at nearby Reanalysis gridpoint 52.5°S, 70°W (Fig. 1), with radiosonde temperatures higher by about 0.2 °C. Both records show warming over 1977–85, about 0.4 °C in the radiosonde and 0.2 °C in the Reanalysis, and none thereafter. This high correlation engenders confidence in the Reanalysis database, at least after 1977.

Inhomogeneities plague both the radiosonde record and the Reanalysis database. The International Geophysical Year (1957–58) inspired increases in the quantity and quality of radiosonde data, and observation times changed 1 June 1957 from 0300 and 1500 UTC, to 0000 and 1200 UTC (Kistler et al., 2001; Angell, 1988). Severe biases in the humidity record prior to about 1975 resulted from the evolution of instrumentation and recording methods (Section 4 of Rasmussen et al., 2001) including some due to changes in sensor design and one due to inadequate shielding from solar radiation, which caused aberrantly low daytime readings. The upper-air database for southern latitudes is afflicted by the scarcity of radiosonde stations, especially over the southeast Pacific Ocean. Radiosondes were established at Puerto Montt about 1957 and at Punta Arenas about 1974. Compilation of the Reanalysis database in the southern hemisphere was based on sea surface temperature fields of dubious accuracy and a distribution of sea ice with

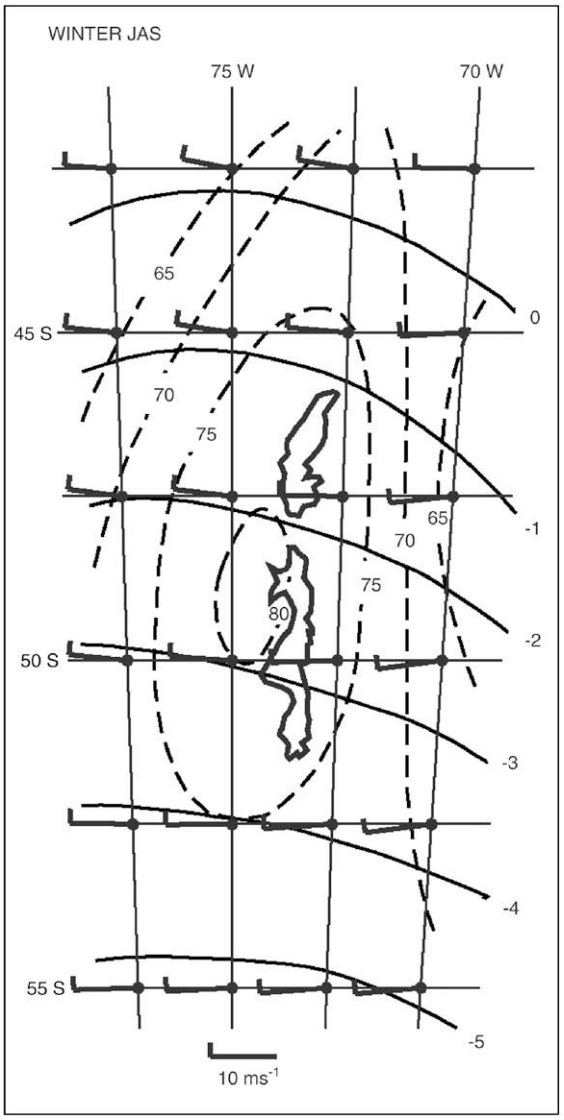

Fig. 3. Mean 1960–99 winter (Jul, Aug, Sep) 850-hPa conditions. Isotherms (solid) are labeled in °C, and dashed isolines are relative humidity labeled in percent. Mean wind speed is proportional to length of staff, not to the barb at the upwind end. Also shown are icefields (Fig. 1).

average seasonal variation instead of actual variations from year to year (Garreaud and Battisti, 1999).

6. Mean 1960–99 upper-air conditions

Although the NCEP–NCAR Reanalysis database begins in 1948, mean values are calculated here only over 1960–99 because of apparent inhomogeneity in the instrumental record in the late 1950s. (Temperature discontinuity is conspicuous in Figs. 12 and 13, shown below.) At 850 hPa, mean winds are strongly westerly, and the temperature gradient is north–northeasterly over the entire region in both winter (Fig. 3) and summer

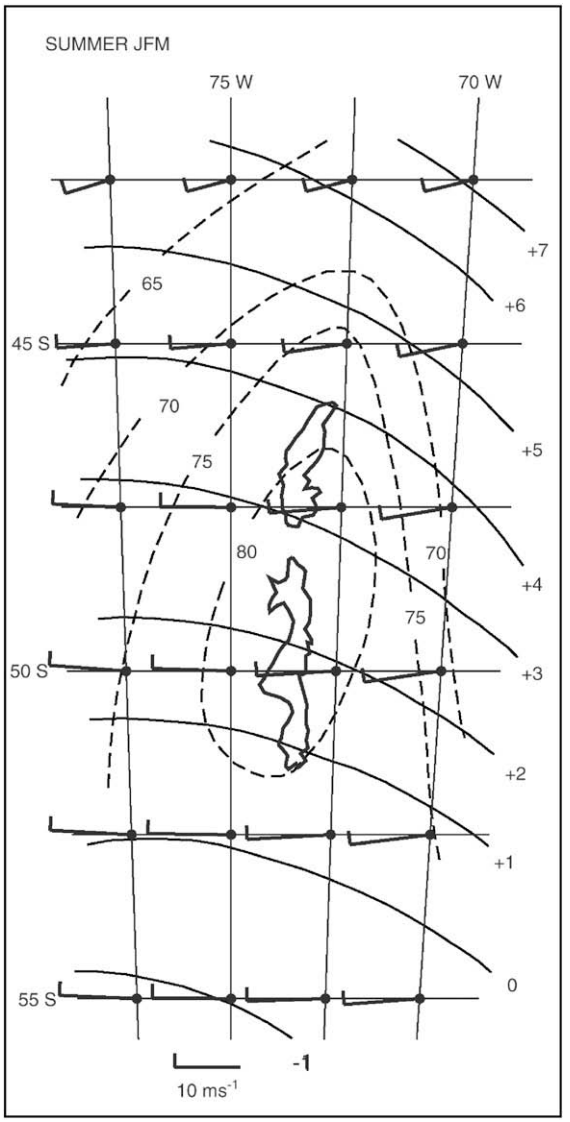

Fig. 4. Same as Fig. 3 but for summer (Jan, Feb, Mar).

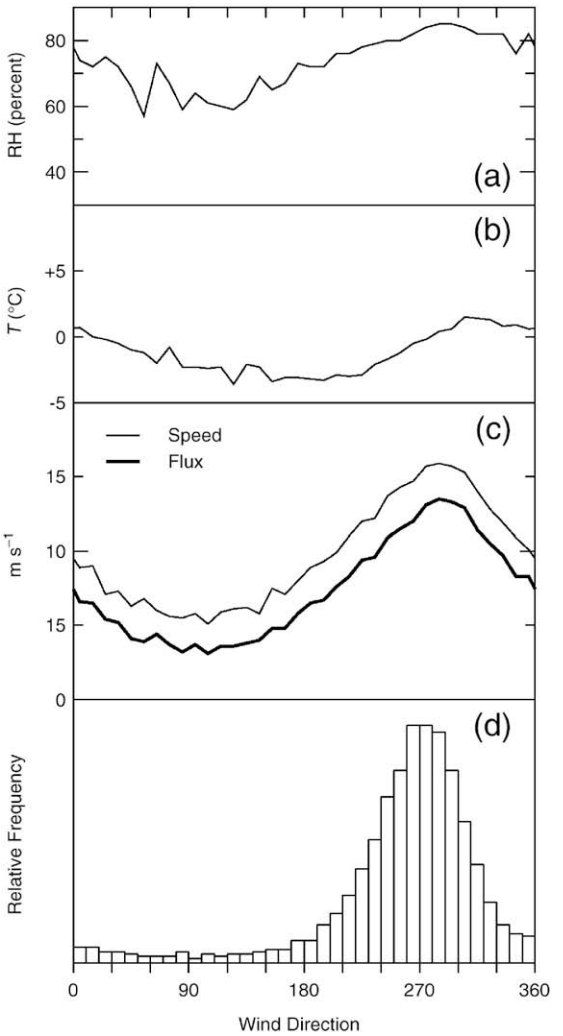

Fig. 5. Mean annual 850-hPa values over 1960–99 as a function of wind direction at 50°S, 75°W. (a) percent relative humidity RH, (b) temperature T in °C, (c) wind speed s and flux (the product s RH), both in m/s, (d) frequency of wind direction.

(Fig. 4). In both seasons the maximum of relative humidity is over the icefields.

The mean 1960–99 wind at Reanalysis gridpoint 50°S, 75°W, just upwind from SPI, is predominantly westerly throughout the year and is strongest, most humid, and warmest when it comes from that direction (Fig. 5), and so is the product of wind speed and RH. This region of strong westerlies has an exceptionally narrow distribution of wind direction. By contrast, at 47.5°N, 125°W over 1960–99 it is much warmer, the wind direction has a much broader peak, at about 220°, and offshore winds are more frequent and much drier. The variables at 50°S, 75°W follow nearly the same distribution when $T \leq +2$ °C as they do for all T.

For two reasons, the critical direction is taken to be $\phi' = 270°$: (1) the prevailing wind is from that direction, and (2) it is also the mean direction of the topographic upslope. In some places in the northern hemisphere, by contrast, the prevailing wind is not in the upslope direction. Precipitation at lowland stations surrounding the Olympic Mountains, a small group with radius about 50 km at 48°N on the west coast of North America, correlates most strongly (Rasmussen et al., 2001) with flow from the southwest, which is the approximate direction of maximum advection of moisture, instead of in the local upslope direction. In the central part of the Cascade Mountains, a north–south trending range 200 km to the east, precipitation correlates best (Hayes et al., 2002) with flow from $\phi' = 256°$, which is nearly perpendicular to the trend of the range. Pandey et al. (1999) found similar results for the California Sierra Nevada, a high range trending nearly northwest–southeast. The salient difference between the two regimes is presumably that air can flow around the small cone-shaped Olympics but cannot flow around the long, linear trend of the other ranges where strong precipitation is produced by the orographic lifting of moist air in proportion to the component of wind perpendicular to the range.

A second assumption in the present analysis is that the 850-hPa snow flux is a good indicator of accumulation on NPI and SPI because of strong positive correlation between snowfall amounts at different elevations z. The 850-hPa level (at ~1400 m) is within the accumulation areas of most glaciers (Section 2). This assumption was investigated in the case of South Cascade Glacier (Appendix A), where the goodness of fit declines slowly as the elevation at which T is interpolated (to apply the $T \leq +2$ °C criterion) increases above the terminus, with rms error 0.24 m w.e. ($r^2 = 0.84$) for T interpolated at 1650 m at the terminus,

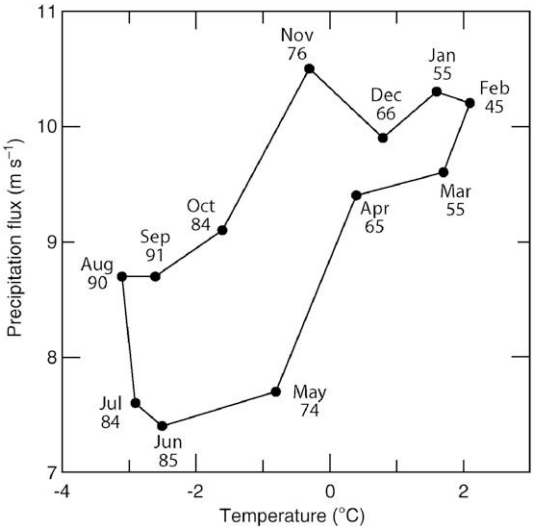

Fig. 7. Mean 1960–99 precipitation flux F in direction 270° vs. temperature, both at 850 hPa at 50°S, 75°W by month. The small number shown for each month is the percent ratio of the snow flux to the precipitation flux.

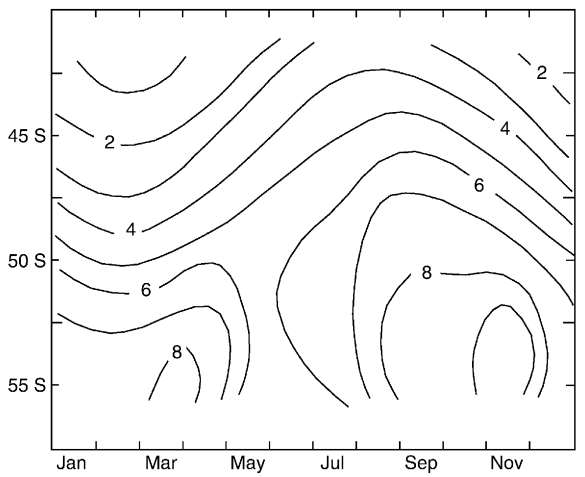

Fig. 6. Seasonal variation of mean 850-hPa snow flux in direction 270° vs. latitude along 75°W, averaged over 1960–99. Contours are labeled in m/s.

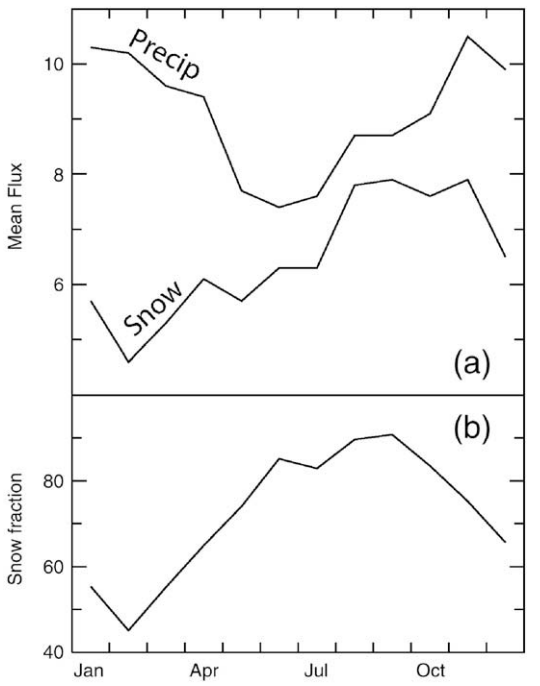

Fig. 8. Seasonal variation of mean precipitation flux F and snow flux (Fig. 6) in direction 270° at 50°S, 75°W over 1960–99. (a) the fluxes in m/s, (b) percent ratio of snow flux to precipitation flux.

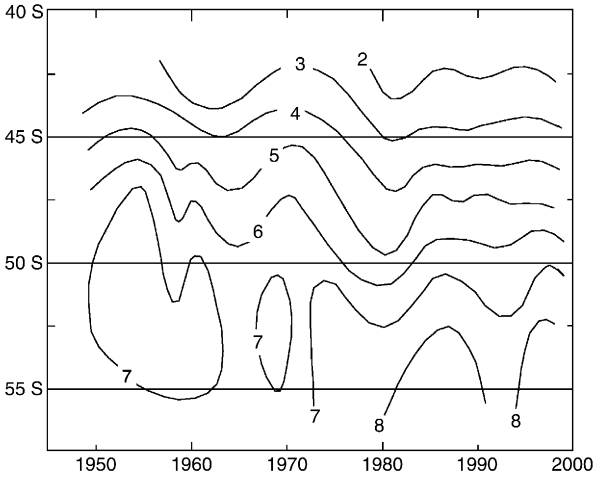

Fig. 9. Three-year running average of mean annual 850-hPa snow flux in direction 270°, along 75°W, over 1949–98. Contours are labeled in m/s.

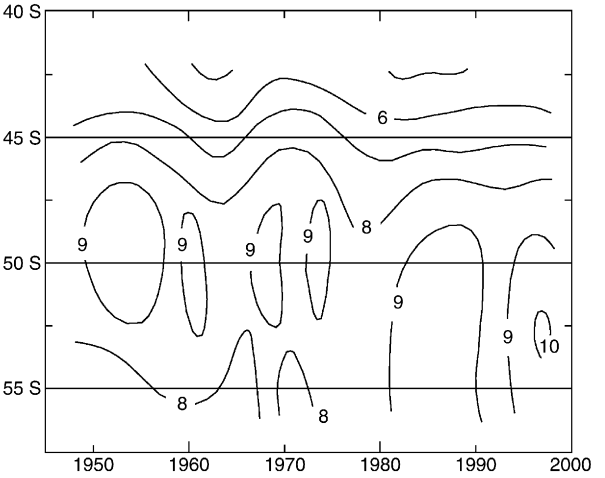

Fig. 11. Three-year running average of mean annual 850-hPa precipitation flux in direction 270°, along 75°W. Contours are labeled in m/s.

compared with 0.28 m w.e. ($r^2=0.80$) for T interpolated at 2150 m. Snowfall at lower z is almost always accompanied by snowfall over the entire glacier, whereas snowfall at higher z is sometimes accompanied by rain at lower z. The correlation over 1959–98 between the calculated snow fluxes using T at 1650 and using T at 2150 m is $r=+0.97$.

Variation with latitude along 75°W of the 1960–99 mean 270° precipitation flux F has a maximum at 50°S, over both the entire year and for the winter months July–September. The ratio of the snow flux (the part of F when $T\leq+2$ °C) to the precipitation flux itself increases with latitude in all seasons and approaches unity at high latitude. Seasonal variation of snow flux by latitude along 75°W (Fig. 6) shows a maximum at high latitude in spring, as demonstrated by the covariance of F and temperature at 50°S, 75°W (Fig. 7). Seasonal variation of the two fluxes there (Fig. 8) shows winter dryness as well as the spring maximum of the snow flux.

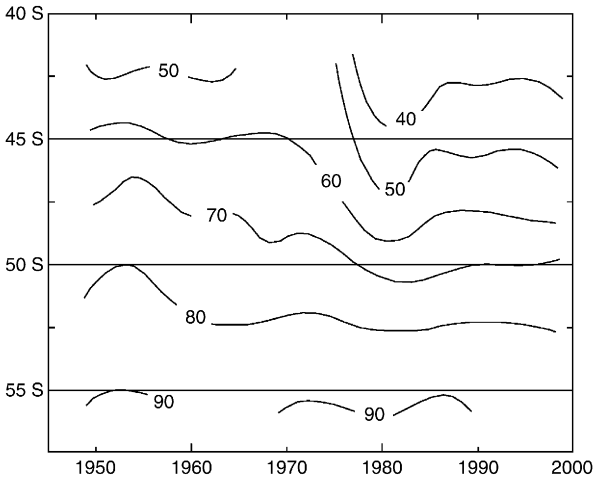

Fig. 10. Three-year running average of ratio of annual snow flux (Fig. 6) to precipitation flux F, both at 850 hPa in direction 270°, along 75°W. Contours are labeled in percent.

7. 1960–99 changes in upper-air conditions

Change between 1960 and the 1990s in the 850-hPa snow flux (U RH in the direction 270° when $T\leq+2$ °C) varied by latitude along 75°W (Fig. 9). It decreased about 20% at 45°S (from 4.2 to 3.2 m/s), decreased about 5% at 50°S (from 7.0 to 6.5 m/s), and increased about 15% at 55°S (from 7.0 to 8.0 m/s). The decrease at 45°S resulted from warming, as shown by the decrease in the snow fraction (Fig. 10) while the precipitation flux changed little (Fig. 11). By contrast, the increase at 55°S is the result of increased precipitation flux and unchanged snow fraction. Warming just below the critical temperature +2 °C diminishes the snow fraction, but at lower temperature does not. The record prior to 1960 is shown to demonstrate what is believed to be

Table 1
Percent correlation r over 1960–99 of snow flux between gridpoints at indicated S latitudes (in degrees) along 75°W. The snow flux F (Eq. (2)) is from direction 270° at 850 hPa when $T\leq+2$ °C

	42.5	45.0	47.5	50.0	52.5	55.0
42.5	100	92	69	25	−18	−49
45.0		100	90	50	1	−36
47.5			100	78	27	−14
50.0				100	73	34
52.5					100	85

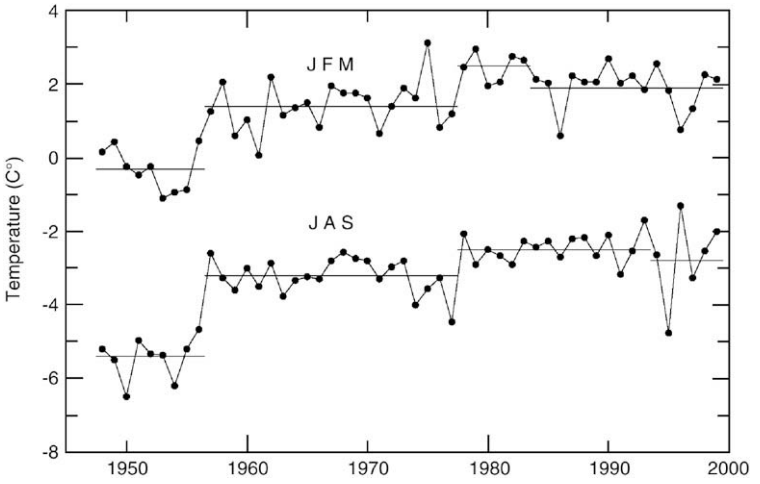

Fig. 12. Time series of seasonal 850-hPa temperature at 50°S, 75°W. Best-fitting piecewise-constant functions have stages 1948–56, 1957–77, 1978–83, and 1984–99 for summer (Jan, Feb, Mar) and 1948–56, 1957–77, 1978–93, 1994–99 for winter (Jul, Aug, Sep). The rms is 0.6°C for each season. The best-fitting constant in a stage is the mean of the values in that stage. Times of discontinuities between stages are determined empirically to give the best fit overall, subject to the constraint that no stage can be less than five years long.

inhomogeneity in the Reanalysis database rather than actual variation. Latitude to latitude correlations between the snow fluxes at 75°W are given in Table 1. Upper-air data in this region is questionable prior to about 1965 when radiosonde stations were established there (Carrasco, written comm., 2004).

At 50°S, there has been little change since 1960 in precipitation flux (Fig. 11), apart from a temporary decrease in the late 1970s. The decrease in snow flux (Fig. 9) is due to warming, as shown by decrease in the ratio of snow flux to precipitation flux (Fig. 10). There does not seem to be a wave in the precipitation flux propagating latitudinally (Fig. 11).

Precipitation decreased at Bahia Felix and Evangelistas (Fig. 1) mainly before 1960 and has no apparent trend until 1985, nor has Punta Arenas (Fig. 5 of Rosenbluth et al., 1995). Increase in precipitation flux at 52.5°S is indicated in Fig. 11, but after about 1990. Precipitation flux calculated from direction 270° is not indicative of precipitation at Punta Arenas, which often comes with easterly flow (Schneider et al., 2003).

Temperature during the accumulation season controls the rain–snow division of precipitation, and during the ablation season controls melt (see, for instance, Braithwaite and Zhang, 2000). In temperate climates, where much precipitation falls just below the critical temperature +2 °C, warming in all seasons is detrimental to glacier mass balance: it decreases accumulation and it increases ablation. The record of both winter and summer 850-hPa temperatures at 50°S, 75°W (Fig. 12) have an abrupt rise of ~2 °C in the late 1950's, which is believed to reflect a discontinuity in observational methods, and a rise of ~0.5 °C since then. The increase in the 1970s is accompanied by increases in global atmospheric surface temperatures (Trenberth et al., 2002), in sea surface temperature in the NE Pacific as part of the Pacific Decadal Oscillation (Hare and Mantua, 2000), and in winter upper-air temperatures in western North America (Rasmussen and Conway, 2004).

This late-1950s feature is present in the summer record (Fig. 13) for other gridpoints along 75°W. The record at 47.5°N, 125°W shows similar warming since 1960 in both seasons and changes in the 1950s of magnitude comparable to those over southern South America but of opposite sign: summer cooling and winter warming. At 47.5°N, 125°W there is about twice

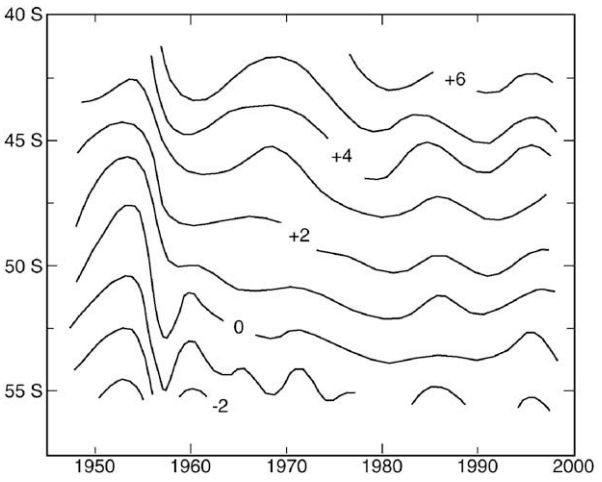

Fig. 13. Three-year running average of 850-hPa summer (Jan, Feb, Mar) temperature vs. latitude along 75°W. Contours are labeled in °C.

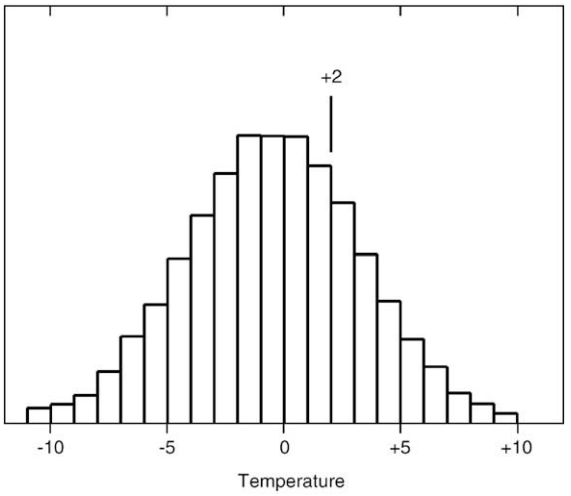

Fig. 14. Frequency distribution of precipitation flux in direction 270° versus 850-hPa temperature (°C) at 50°S, 75°W in 1 °C increments, averaged over 1948–99. The [−11, −10) bar includes all of the cold tail down to −16 °C, and the [+9, +10) bar includes all of the warm tail up to +17 °C.

as much variation, both between the two seasons and from year-to-year within each season.

Sensitivity to temperature change of the calculated snow flux at 50°S, 75°W is slightly asymmetric because most precipitation flux F is at $T<+2$ °C (Fig. 14). The fraction of the distribution in $+2 \le T<+3$ °C is 0.079 and in $+1 \le T<+2$ °C is 0.092. Thus, all other things remaining the same, decrease of snowfall upon +1 °C warming would be 9%, whereas the increase upon +1 °C cooling would be 8%.

There are several reasons why warming at 850 hPa appears to differ from temperature trends at surface stations. One is that there are few stations in the region with long records, so that surface temperatures are not well sampled. Another is that the diurnal range of temperature is much greater at the surface than in the free atmosphere, and trends in surface temperature, which are positive at some stations, negative at others, are caused mainly by changes in minimum temperatures (Rosenbluth et al., 1997).

8. Conclusions

Investigating the response of glaciers to upper-air conditions is hampered by the scarcity of measurements of mass balance on the icefields as well as of precipitation at nearby sites. Relations between upper-air conditions and precipitation that were developed for sites in North America also work on the west coast of southern Chile but not nearly as well. In North America, data from the NCEP–NCAR Reanalysis database give comparable results to those from radiosonde measurements.

There appear to be aberrant 850-hPa temperatures in the 1950s at Reanalysis gridpoints over southern South America. Since then, warming at 850 hPa at 50°S, the latitude of the icefields, has been about 0.5 °C both winter and summer, although it is not possible to discern whether the evidence for it is real or is due to data inhomogeneities. Such warming, if it extended over the elevation range of the icefields, would have both increased the ablation and decreased the fraction of precipitation falling as snow. The calculated 850-hPa precipitation flux at that latitude lacks noticeable trend over 1960–99, indicating that the decline of snowfall has been due to warming rather than drying.

In November–December 1993, Takeuchi et al. (1995) determined that in the ablation area of two glaciers on the east side of the southern end of SPI, melt increased by an average of ~10 mm w.e. per day for a +1 °C change in temperature. If that rate prevailed over an ablation season of 100 days (as an approximation of the effect of a varying rate over an actual longer season), the total would be 1 m for a +1 °C change. Not considering the apparently aberrant record of the 1950s, summer (January–March) 850-hPa temperature at 50°S, 75°W has increased by about 0.5 °C over the past 40 years (Fig. 13). The product of this warming rate and the observed sensitivity indicates cumulative increase since 1960 of 0.5 m w.e. per year of melt in the ablation area of the icefields.

When the cumulative increase over 1960–99 of 0.5 m w.e. per year of melt is applied only to 4100 km^2 of the ablation area of SPI, along with a 5% reduction to the 6.7 m w.e. annual accumulation over 8700 km^2 of its accumulation area, the resultant is −0.4 m w.e. per year over the entire icefield. Including some reduced accumulation in the ablation area and some increased melt in the accumulation area would make the resultant more negative. Perspective for the magnitude for these changes is given by Dyurgerov and Meier (1997, their Tables 2 and 3), who calculate −0.3 m w.e. per year mass balance over 1961–90 for glaciers in Canada and the U. S. at comparable latitude to the Patagonia icefields. Kerr and Sugden (1994, p. 265) calculate that at the latitude of NPI, the ELA will rise about 150 m for 1 °C warming, including effects of both enhanced melt and diminished snow-to-rain ratio, and by about 30 m for 10% reduction of precipitation.

If the snow flux analysis is valid, accumulation on the icefields has decreased about 5% over the past 40 years, more at NPI than at SPI. Over the same period, according to the 850-hPa temperature record,

summer warming has enhanced ablation. Rasmussen and Conway (2003) determined that for a glacier in a marine climate at 48.4°N, the sensitivity of summer balance to warming is −0.5 m/°C. Because mass loss of the icefields has prevailed since at least 1870 (Harrison and Winchester, 2000), however, the decline in mass balance resulting from these two 40-year trends represents only an acceleration of the long-term trend of adjusting to climate change since the Little Ice Age. For this reason, the apparent increase in snow flux at 55°S (Fig.9) does not necessarily indicate that glaciers there are growing.

Acknowledgments

This work was supported by NASA grant 1215388 and U.S. NSF grant OPP-0240861. G. Casassa provided precipitation data as well as much useful consultation on prior glaciological research in Patagonia. We thank E. Recker for retrieval of the NCEP–NCAR Reanalysis data and A. Rivera for assistance with Figure 1. Comments by J. Carrasco, D. Kilham, and A. Rivera much improved the manuscript.

Appendix A. Model results at 48°N

When twice-daily radiosonde observations were used, the model estimated 30-day precipitation P at Forks, 12 km E of Quillayute (at 47.95°N, 124.55°W near the Pacific coast), with accuracy $r^2=0.88$ (Rasmussen et al., 2001), and at Longmire, 225 km SE of Quillayute, with accuracy $r^2=0.78$ (Hayes et al., 2002). For Longmire and four other stations near it on the west side of the Cascade Mountains, the model underestimated total precipitation for the 143-day period ending 30 April 1997 with relative errors $(P^*-P)/P$ ranging from −0.15 to −0.02, whereas MM5 (the nonhydrostatic version of the Pennsylvania State University, National Center for Atmospheric Research mesoscale model) had errors ranging from −0.25 to +0.35 (Colle et al., 1999). MM5 produces estimates on a 12-km square grid, facilitating interpolation, whereas estimates from the flux model are confined to the sparse array of observing stations because, unlike MM5, it must be calibrated for α (Eq. (1)) and ϕ' (Eq. (2)) from each station's precipitation record.

October–September runoff R in the Cedar River at Cedar Falls, 220 km ESE of Quillayute, is estimated from the precipitation flux F by $R=\beta F+\gamma$ with accuracy $r^2=0.82$ over the 30 water years 1967–96. Here β corresponds to P/F and $\gamma<0$ accounts for annual evapotranspiration. Using only October–April F does slightly better ($r^2=0.83$) than using the total October–September F does; only about one sixth of the annual precipitation in this region falls in May–September and much of that is lost to evapotranspiration during the warm growing season. The basin, near Longmire, has an area of 105 km^2 and ranges in elevation from 500 to 1600 m above sea level. The specific runoff R is 2100 mm and $\gamma=-600$ mm.

October–April winter balance at South Cascade Glacier is estimated by $b_w=\lambda F+\delta$, in which F is used from only those days on which temperature T interpolated at 1650 m between the 850 and 700 hPa levels is less than +2 °C (Rasmussen and Conway, 2001). Here λ corresponds to P/F on those days when precipitation falls on the glacier as snow, and $\delta<0$ corresponds to ablation during the accumulation season. Most precipitation on the glacier falls as snow, with ~3 m w.e. accumulating each winter at the head of the glacier; annual ablation at the terminus usually exceeds 8 m w.e. It is a small, north facing, temperate glacier on the crest of the North Cascade Range, 260 km ENE of Quillayute with an elevation range of 1630 to 2130 m and area of 2.0 km^2. Over 1959–98, the model estimated winter balance with rms error 0.24 m w.e. ($r^2=0.84$).

Table A-1
Comparison of model results: Reanalysis vs. radiosonde databases. Times 0000 and 1200 are UTC. Precipitation P and October–September runoff R in millimeters, glacier winter balance b_w in water-equivalent meters. Period is 1966–96 for P and R, 1959–98 for b_w

Variable	Radiosonde 0000 and 1200			Radiosonde 1200			Reanalysis 1200		
	rms	r^2	ϕ'	rms	r^2	ϕ'	rms	r^2	ϕ'
Forks 1-day P	11.1	0.51	238°	11.1	0.51	231°	10.4	0.57	231°
Forks 30-day P	67.7	0.88	230°	76.9	0.86	228°	69.9	0.87	231°
Longmire 1-day P	8.9	0.36	262°	9.8	0.22	265°	9.4	0.28	269°
Longmire 30-day P	61.8	0.78	259°	68.9	0.73	256°	65.3	0.76	260°
Cedar River R	201	0.82	258°	236	0.75	255°	253	0.71	265°
South Cascade b_w	0.24	0.84	263°	0.26	0.82	262°	0.29	0.78	271°

Table A-2
Comparison of databases on days when Forks had at least 10 mm precipitation, over 1967–98: R is Reanalysis, Q is radiosonde, ($\Delta=R-Q$), time is 1200 UTC. Wind direction, speed (meters per second), relative humidity (percent) all at 850 hP

Variable		JFM	AMJ	JAS	OND	Annual
Wind speed	R	14.2	10.9	9.7	13.7	13.1
	Q	15.1	11.7	10.5	15.0	14.1
	Δ	−0.9	−0.8	−0.8	−1.3	−1.0

Table A-2 (*continued*)

Variable		JFM	AMJ	JAS	OND	Annual
Wind direction	*R*	223°	222°	225°	227°	224°
	Q	214°	210°	213°	218°	215°
	Δ	+9	+12	+12	+8	+9
Relative humidity	*R*	85	87	85	82	84
	Q	89	90	88	89	89
	Δ	−4	−3	−3	−7	−5

References

Angell, J.K., 1988. Variations and trends in tropospheric and stratospheric global temperatures, 1958–87. J. Climate 1, 1296–1313.

Aniya, M., Wakao, Y., 1997. Glacier variations of Hielo Patagonico Norte, Chile, between 1944/45 and 1995/96. Bull. Glacier Res. 15, 11–18.

Aniya, M., Sato, H., Naruse, R., Skvarca, P., Cassasa, G., 1996. The use of satellite and airborne imagery to inventory outlet glaciers of the Southern Patagonia Icefield, South America. Photogramm. Eng. Remote Sensing 62, 1361–1369.

Aniya, M., Dhakal, A.S., Park, S., Naruse, R., 2000. Variations of Patagonian glaciers, South America, using RADARSAT and LANDSAT images. Can. J. Remote Sens. 26 (6), 501–511.

Aristarain, A.J., Delmas, R.J., 1993. Firn-core study from the southern Patagonia ice cap, South America. J. Glaciol. 39 (132), 249–254.

Braithwaite, R.J., Zhang, Y., 2000. Sensitivity of mass balance of five Swiss glaciers to temperature changes assessed by tuning a degree–day model. J. Glaciol. 46 (152), 7–14.

Carrasco, J.F., Casassa, G., Rivera, A., 2002. Meteorological and climatological aspect of the southern Patagonia icefield. In: Casassa, G., Sepulveda, F., Sinclair, R. (Eds.), The Patagonia Icefields. Kluwer-Plenum, New York, pp. 29–41.

Casassa, G., Rivera, A., Aniya, M., Naruse, R., 2002. Current knowledge of the southern Patagonia icefield. In: Casassa, G., Sepulveda, F., Sinclair, R. (Eds.), The Patagonia Icefields. Kluwer-Plenum, New York, pp. 67–83.

Colle, B.A., Westrick, K.J., Mass, C.F., 1999. Evaluation of MM5 and Eta-10 precipitation forecasts over the Pacific Northwest during the cool season. Weather Forecast. 14, 137–154.

Dyurgerov, M.B., Meier, M.F., 1997. Year-to-year fluctuations of global mass balance of small glaciers and their contribution to sea level changes. Arct. Alp. Res. 29 (4), 392–402.

Enomoto, H., Nakajima, C., 1985. Recent climate fluctuations in Patagonia. In: Nakajima, C. (Ed.), Glaciological studies in Patagonia Northern Icefield, 1983–1984. Jap. Soc. Snow and Ice, pp. 7–14.

Escobar, F., Fernando, V., Garin, C., 1992. Water balance in the Patagonia icefield. In: Naruse, R., Aniya, M. (Eds.), Glaciological Researches in Patagonia, 1990. Jap. Soc. Snow and Ice, pp. 109–119.

Fukami, H., Naruse, R., 1987. Ablation of ice and heat balance of Soler Glacier, Patagonia. Bull. Glacier Res. 4, 37–42.

Garreaud, R.D., Battisti, D.S., 1999. Interannual ENSO and interdecadal ENSO-like variablilty in the southern hemisphere tropospheric circulation. J. Climate 12, 2113–2123.

Godoi, M.A., Shiraiwa, T., Kohshima, S., Kubota, K., 2002. Firn-core drilling operation at Tyndall Glacier, Southern Patagoia Icefield. In: Casassa, G., Sepulveda, F., Sinclair, R. (Eds.), The Patagonia Icefields. Kluwer-Plenum, New York, pp. 149–156.

Hare, S.R., Mantua, N.J., 2000. Empirical evidence for North Pacific regime shifts in 1977 and 1989. Prog. Oceanogr. 47, 103–145.

Harrison, S., Winchester, V., 2000. Nineteenth- and twentieth-century glacier fluctuations and climatic implications in the Arco and Colonia Valleys, Hielo Patagonia Norte, Chile. Arct. Antarct. Alp. Res. 32 (1), 55–63.

Hayes, P.S., Rasmussen, L.A., Conway, H., 2002. Estimating precipitation in the central Cascades of Washington. J. Hydrometeorol. 3, 335–346.

Hulton, N.R., Sugden, D.E., 1995. Modeling mass balance on former maritime ice caps: a Patagonia example. Ann. Glaciol. 21, 304–310.

Ibarzabal y DonAngelo, T., Hoffmann, J.A.J., Naruse, R., 1996. Recent climate changes in southern Patagonia. Bull. Glacier Res. 14, 29–36.

Johannesson, T., Sigurdsson, O., Laumann, T., Kennett, M., 1995. Degree–day glacier mass-balance modeling with applications to glaciers in Iceland, Norway and Greenland. J. Glaciol. 41 (138), 345–358.

Kalnay, E., et al., 1996. The NCEP-NCAR 40-year reanalysis project. Bull. Am. Meteorol. Soc. 77 (3), 437–471.

Kerr, A., Sugden, D.E., 1994. The sensitivity of the south Chilean snowline to climatic change. Clim. Change 28, 255–272.

Kistler, R., et al., 2001. The NCEP-NCAR 40-year reanalysis: monthly means CD-ROM and documentation. Bull. Am. Meteorol. Soc. 82 (2), 247–267.

Kobayashi, S., Saito, T., 1985. Meteorological observations on Soler Glacier. In: Nakajima, C. (Ed.), Glaciological studies in Patagonia Northern Icefield, 1983–1984. Jap. Soc. Snow and Ice, pp. 32–36.

Koizumi, K., Naruse, R., 1992. Measurements of meteorological conditions and ablation at Tyndall Glacier, southern Patagonia, in December 1990. Bull. Glacier Res. 10, 79–82.

Laumann, T., Reeh, N., 1993. Sensitivity to climate change of the mass balance of glaciers in southern Norway. J. Glaciol. 39 (133), 656–665.

Matsuoka, K., Naruse, R., 1999. Mass balance features derived from a firn core at Hielo Patagonico Norte, South America. Arct. Alp. Res. 31 (4), 333–340.

Mercer, J.H., 1965. Glacier variations in southern Patagonia. Geogr. Rev. 55 (5), 390–413.

Naruse, R., Skvarca, P., Takeuchi, Y., 1997. Thinning and retreat of Glacier Upsala, and an estimate of annual ablation changes in southern Patagonia. Ann. Glaciol. 24, 38–42.

Oerlemans, J., 1993. A model for the surface balance of ice masses: part 1. Alpine Glaciers. Z. Gletsch.kd. Glazialgeol. 27–28 (1991–1992), 63–83.

Ohata, T., Enomoto, H., Kondo, H., 1985. Characteristics of ablation at San Rafael Glacier. In: Nakajima, C. (Ed.), Glaciological studies in Patagonia Northern Icefield, 1983–1984. Jap. Soc. Snow and Ice, pp. 37–45.

Pandey, G.R., Cayan, D.R., Georgakakos, K.P., 1999. Precipitation structure in the Sierra Nevada of California during winter. J. Geophys. Res. 104, 12019–12030.

Rasmussen, L.A., Conway, H., 2001. Estimating South Cascade Glacier mass balance from a distant radiosonde and comparison with Blue Glacier. J. Glaciol. 47 (159), 579–588.

Rasmussen, L.A., Conway, H., 2003. Using upper-air conditions to estimate South Cascade Glacier (USA) summer balance. J. Glaciol. 49 (166), 454–462.

Rasmussen, L.A., Conway, H., 2004. Climate and glacier variability in Western North America. J. Climate 17 (9), 1804–1815.

Rasmussen, L.A., Conway, H., Hayes, P.S., 2000. The accumulation regime of Blue Glacier, U.S.A., 1914–96. J. Glaciol. 46 (153), 326–334.

Rasmussen, L.A., Conway, H., Hayes, P.S., 2001. Estimating Olympic Peninsula precipitation from upper air wind and humidity. J. Geophys. Res. 106, 1493–1501.

Rignot, E., Rivera, A., Casassa, G., 2003. Contribution of the Patagonia Icefields of South America to sea level rise. Science 302, 434–437.

Rivera, A., Acuna, C., Casassa, G., Bown, F., 2002. Use of remotely sensing and field data to estimate the contribution of Chilean glaciers to eustatic sea level rise. Ann. Glaciol. 34, 367–372.

Rosenbluth, B., Casassa, G., Fuenzalida, H.A., 1995. Recent climatic changes in western Patagonia. Bull. Glacier Res. 13, 127–132.

Rosenbluth, B., Fuenzalida, H.A., Aceituno, P., 1997. Recent temperature variations in southern South America. Int. J. Climatol. 17, 67–85.

Schneider, C., Gies, D., 2004. Effects of ENSO on southern South America revealed from NCEP/NCAR Reanalysis data. Int. J. Climatol. 24, 1057–1076.

Schneider, C., Glaser, M., Kilian, R., Santana, A., Butorovic, N., Casassa, G., 2003. Weather observations across the southern Andes at 53°S. Phys. Geogr. 24 (2), 97–119.

Shiraiwa, T., et al., 2002. High net accumulation at camp Hielo Patagonia Sur, South America, revealed by analysis of a 45.97 m long ice core. Ann. Glaciol. 35, 84–90.

Skvarca, P., De Angelis, H., 2002. Fifteen-year changes of Southern Patagonia Icefield glaciers, Argentina–Chile, detected from Landsat TM mosaics. In: Saints, J. (Ed.), Proceedings of the 29th International Symposium on Remote Sensing of the Environment. ISRSE Organizing Committee.

Takeuchi, Y., Naruse, R., Satow, K., 1995. Characteristics of heat balance and ablation on Moreno and Tyndall glaciers, Patagonia, summer 1993/94. Bull. Glacier Res. 13, 45–56.

Takeuchi, Y., Naruse, R., Skvarca, P., 1996. Annual air-temperature measurements and ablation estimate at Moreno glacier, Patagonia. Bull. Glacier Res. 14, 23–28.

Takeuchi, Y., Naruse, R., Satow, K., Ishikawa, N., 1999. Comparison of heat balance characteristics at five glaciers in the Southern Hemisphere. Glob. Planet. Change 13, 201–208.

Trenberth, K.E., Caron, J.N., Stepaniak, D.P., Worley, S., 2002. Evolution of El Nino—Southern Oscillation and global atmospheric surface temperatures. J. Geophys. Res. 107 (AAC5), 1–19.

Warren, C.R., Sugden, D.E., 1993. The Patagonian Icefields: a glaciological review. Arct. Alp. Res. 25, 316–331.

Yamada, T., 1987. Glaciological characteristics revealed by 37.6-m deep core drilled at the accumulation area of San Rafael Glacier, North Patagonia Icefield. Bull. Glacier Res. 4, 59–67.